Article

Characterization and Photocatalytic Performance of Newly Synthesized ZnO Nanoparticles for Environmental Organic Pollutants Removal from Water System

Vesna Despotović [1,†], Nina Finčur [1,†], Sabolč Bognar [1], Daniela Šojić Merkulov [1,*], Predrag Putnik [2,*], Biljana Abramović [1] and Sanja Panić [3]

1   Department of Chemistry, Biochemistry and Environmental Protection, University of Novi Sad Faculty of Sciences, Trg Dositeja Obradovića 3, 21000 Novi Sad, Serbia; vesna.despotovic@dh.uns.ac.rs (V.D.); nina.fincur@dh.uns.ac.rs (N.F.); sabolc.bognar@dh.uns.ac.rs (S.B.); biljana.abramovic@dh.uns.ac.rs (B.A.)
2   Department of Food Technology, University North, Trg dr. Žarka Dolinara 1, 48000 Koprivnica, Croatia
3   Faculty of Technology, University of Novi Sad, Bulevar cara Lazara 1, 21000 Novi Sad, Serbia; sanjar@tf.uns.ac.rs
*   Correspondence: daniela.sojic@dh.uns.ac.rs (D.Š.M.); pputnik@alumni.uconn.edu (P.P.)
†   These authors contributed equally to this work.

Abstract: Most countries are facing problems of environmental pollution due to toxic organic pollutants being discharged into the environment from various man-made sources. Heterogeneous photocatalysis is a possible solution for the mentioned problem, and it has been widely applied for the removal of pollutants from aqueous solutions, thanks to its high removal efficiency and environmental friendliness. Among the commonly used metal oxides, ZnO has attracted researchers' interests due to its ecofriendly and nontoxic nature. In this work, ZnO nanoparticles (ZnO-NPs) were prepared by the precipitation method from water (w) and ethanol solutions of the corresponding metal precursors (zinc–acetate dihydrate, A_ZnO, and zinc–nitrate hexahydrate, N_ZnO) followed by calcination at different temperatures. The structure and morphology of the prepared catalysts were characterized by different techniques (XRD, BET, and SEM). Based on the XRD results, it can be seen that the synthesized NPs possess high purity. Furthermore, at a higher calcination temperature, a higher crystal size was observed, which was more intense in the case of the ethanol solution of the precursors. The BET analysis showed macropores at the surface and also indicated that the increased temperature led to decreased surface area. Finally, SEM images showed that in the case of the water precursor solution, an irregular, rod-like shape of the NPs was observed. The photocatalytic properties of newly synthesized ZnO-NPs exposed to simulated sunlight were examined during the removal of pesticide clomazone (CLO) and the antidepressant drug amitriptyline (AMI). ZnO-NPs prepared by the precipitation method from the water solution of zinc–acetate dihydrate and calcined at 500 °C (A_ZnOw_500) showed the highest performance under simulated sunlight. Furthermore, the activity of A_ZnOw_500 and N_ZnOw_500 catalysts in the removal of three organic pollutants from water—two pesticides (sulcotrione (SUL) and CLO) and one pharmaceutical (AMI)—was also compared. Results showed that decreased photocatalytic activity was observed in the presence of N_ZnOw_500 NPs in all investigated systems. Finally, the effect of the initial pH was also examined. It was found that in the case of CLO and SUL, there was no influence of the initial pH, while in the case of AMI the k_{app} was slightly increased in the range from pH ~7 to pH ~10.

Keywords: ZnO; chemical precipitation; metal precursors; removal efficiency; pesticides; pharmaceuticals

1. Introduction

The release of pollutants, such as pesticides and pharmaceutically active compounds, in the environment is a global concern and has attracted much attention from the public and the scientific community, due to their adverse impact on human health, plants, soil,

and aquatic systems. Many studies confirmed the toxicological effects of these pollutants, even at low concentrations, which becomes further complicated and outstanding if they are present as a mixture [1,2].

The presence of pesticides in water has received much attention from researchers because of their prolonged persistence in the aqueous environment and because of the threat they pose to human health. Namely, these pollutants enter the human body through food and drinking water [3]. In addition, the results of degradation processes (biotic and abiotic) show that pesticides can be transformed into several products that may have higher toxicity or persistence than their parent compounds [4–9].

Clomazone (CLO, 2-[(2-chlorophenyl)methyl]-4,4-dimethyl-1,2-oxazolidin-3-one), belongs to the class of oxazolidinones, and it is widely used in agriculture to control weeds for many crops, notably soybeans, cotton, and tobacco. This herbicide is highly effective and can cause contamination due to its high water solubility (1100 mg/L) and long half-life dissipation, averaging from 28 to 84 days. These properties indicate that CLO is primarily found in the water ecosystem phase [10–12].

Sulcotrione (SUL, 2-(2-chloro-4-(methylsulfonyl)benzoyl)cyclohexane-1,3-dione) is a foliar post-emergence herbicide, used to control barnyard grass and dicotyledonous weeds in maize fields [13]. Due to its high water solubility (165 mg/L) and mobility (organic carbon adsorption coefficient, Koc of 36 mL/g), SUL has great potential for leaching [14–16]. Furthermore, SUL was detected in water from the Klodnica River in Poland in a concentration of 57 μg/L, which is significantly above the maximum allowed value for pesticide in drinking water (0.1 μg/L) [17].

Pharmaceuticals are designed to elicit a precise biological response, and their presence in water, even at low concentrations, may pose a threat to human health and ecosystems [18–20]. A commonly prescribed group of pharmaceuticals is psychiatric drugs, which include anxiolytics, antidepressants, selective serotonin re-uptake inhibitors, tricyclic antidepressants, hypnotics, sedatives, and others [21]. These kinds of pharmaceuticals can affect the central nervous system and disrupt neuro-endocrine signaling [22].

Amitriptyline hydrochloride (AMI, 3-(10,11-dihydro-5*H*-dibenzo[*a*,*d*][7]annulen-5-ylidene)-*N*,*N*-dimethylpropan-1-amine hydrochloride) is a tricyclic antidepressant from the class of dibenzocycloheptadien, which is most commonly used in the treatment of depression, including clinical/endogenous depression, as well as in the treatment of insomnia, migraine, etc. [23]. AMI is found in wastewaters [24,25] and surface waters [26,27], as well as in drinking water [28]. Since AMI occurs in the environment, it is necessary to thoroughly examine its stability in the aquatic environment and the possibility of its elimination.

In recent years, heterogeneous photocatalysis using nano-sized semiconductors has been considered a promising and innovative solution for water purification due to its unique chemical, optical, electrical, and non-toxic properties [29–33].

The photocatalytic degradation of CLO was investigated in aqueous TiO_2 Degussa P25 suspension using UV, visible, or natural sunlight. The results of our study clearly indicated that UV/TiO_2 treatment can efficiently eliminate CLO from water [34]. In our previous study, the obtained results showed that the photocatalytic treatment with TiO_2 and UVA irradiation can efficiently eliminate SUL alone and in its commercial formulation Tangenta® from water [35]. A comprehensive study of the removal of pharmaceutical (AMI) and pesticides (SUL, and CLO) from double distilled (DDW) and environmental waters was conducted using bare TiO_2 nanoparticles and TiO_2/polyaniline (TP-50, TP-100, and TP-150) nanocomposite powders. The results indicated that the efficiency of the photocatalytic degradation of AMI was higher in environmental waters—rivers and lakes—in comparison to DDW. On the contrary, the degradation efficacies of SUL and CLO were lower in environmental waters [36].

Among the commonly used metal oxides, ZnO has attracted researchers' interests due to its eco-friendly and non-toxic nature [37]. Moreover, ZnO has emerged as a competent photocatalyst because it is able to generate H_2O_2 more efficiently compared to other metal

oxide nanostructures [38]. Compared to commercially available TiO_2, ZnO has shown higher photocatalytic performance, due to its significant light absorption efficacy along with its many active sites and high surface reactivity. The structure, particle size, particle size distribution, and morphology influence the properties of ZnO. In general, the specific surface area and surface defects in metal-oxide-based photocatalysts play a vital role during degradation reactions [39,40]. These parameters strongly depend on the preparation method and experimental conditions. The effect of typical parameters (type of metal precursor, solution concentration, temperature, agitation time, etc.) on the physicochemical properties of the synthesized ZnO nanoparticles has been examined, excluding the influence of the solvent type (mediating solvent), which has not been investigated in detail. To synthesize ZnO semiconductor, various methods have been used, including the solid-state method [41], the chemical precipitation method [42,43], the sol-gel technique [44], the ultrasonication method [45], the direct heating of the salt precursor [46], and the organometallic synthesis route [47]. Depending on the applied technique, the physicochemical properties of the nanoparticles can be tailored, leading to the desired sizes, morphologies, texture, surface properties and crystalline structure of the nanoparticles. Besides being controllable in terms of the preferred characteristics of the particles, a certain synthesis method can be favored in relation to the others if it can be portrayed by reproducibility, cost effectiveness, scalability, simple operation, and mild operational conditions. The precipitation technique is a chemical synthesis method widely used due to its many advantages, i.e., it is a low-cost, controllable, reproducible, and simple technique to produce various types of ZnO nanoparticles [42,43].

In this paper, the efficiency of newly synthesized ZnO nanoparticles exposed to simulated sunlight (SS) was examined in the removal of three rarely studied organic pollutants from water—two pesticides (CLO and SUL) and one pharmaceutical (AMI). In order to study the kinetics of the photocatalytic reaction, liquid chromatography was used. Newly synthesized photocatalysts were prepared by the precipitation method from water and ethanol solutions of the corresponding metal precursors (acetate and nitrate) followed by calcination at different temperatures. The structure and morphology of the synthesized catalysts were characterized by different techniques and correlated with their performance in the photocatalytic processes. Therefore, this paper can significantly contribute to better understanding the relationship between the applied synthesis conditions and the obtained morphological, structural and textural properties of ZnO nanoparticles in order to tailor these properties by the appropriate selection of the synthesis parameters.

2. Materials and Methods

2.1. Synthesis of ZnO Nanoparticles (ZnO-NPs)

The ZnO photocatalysts were synthesized by the precipitation method from water (ZnOw) and ethanol (ZnOe) solutions of the corresponding two most common metal precursors, zinc–acetate dihydrate (ACS reagent, ≥98%, Sigma-Aldrich, USA) and zinc–nitrate hexahydrate (reagent grade, 98%, Sigma-Aldrich, USA). Detailed information on the synthesis can be found in the Supplementary Material. The obtained samples of ZnO-NPs were labeled as X_ZnOw/e_Y, where X and Y designate the type of metal precursor (A for acetate and N for nitrate) and the applied calcination temperature, respectively. Due to comparison, the as-synthesized ZnO-NPs, prepared without the calcination step (A_ZnOw and A_ZnOe), were characterized, and their photocatalytic performance was tested as well.

2.2. Materials Characterization

The textural characterization, structure and surface morphology of ZnO-NPs were characterized by different techniques: X-ray diffraction (XRD), Brunauer–Emmett–Teller (BET) surface area analysis [48] and scanning electron microscopy (SEM). Detailed information on the characterization can be found in the Supplementary Material.

2.3. Measurements of Photocatalytic Activity

The photocatalytic efficiencies of the newly synthesized ZnO nanoparticles were evaluated in the removal of two herbicides, CLO (98.8%, Sigma-Aldrich, USA) and SUL (≥98%, Sigma-Aldrich, USA), and an antidepressant, AMI (≥98%, Sigma-Aldrich, USA), from their aqueous solutions. The removal experiments were performed as previously described by our group [34], and detailed information can be found in the Supplementary Material.

2.4. Analytical Methods

The experimental conditions for ultrafast liquid chromatography with diode array detector (UFLC−DAD), UV energy fluxes, and pH measurements can be found in the Supplementary Material.

Apparent rate constants were calculated with linear and non-linear (exponential) fitting. Non-linear fit gave a better coefficient of determination compared to linear fit, where, in some cases, significant deviations from the straight line were observed. Therefore, further calculations were performed with apparent rate constants obtained by exponential fitting [49]. All experiments were performed in triplicate.

3. Results and Discussion

3.1. Characterization of ZnO Nanoparticles (ZnO-NPs)

The obtained XRD patterns (Figure 1) for all ZnO samples show the same characteristic XRD peaks, indicating the same type of crystal structure.

The sharp intense peaks in all samples can be associated with the hexagonal wurtzite ZnO structure, with the most intense signals at 2θ values of 31.7° (100), 34.4° (002) and 36.2° (101) (COD database code: 9008877, Reference code 96-900-8878). Since no additional reflections were detected, the synthesized photocatalysts can be characterized by high purity. The average crystallite size of the ZnO samples was calculated by the Scherrer equation based on the reflection from 101 plane (Table 1). As the calcination temperature increases, the crystallite size of the ZnO nanoparticles has an increasing trend also, revealing the significant aggregation of the particles imposed by the high-temperature treatment. The influence of the synthesis medium type is more prominent in the case of uncalcined samples compared to their calcined counterparts. The uncalcined ZnOe can be characterized by the smallest crystallites among all synthesized samples. Moreover, the difference in the ZnO particle size prepared at two adjacent calcination temperatures is higher for the samples prepared in ethanol solution compared to the water-originating ones. Such an observation indicates that ethanol, in the role of a catalyst synthesis medium, promotes an increase in the average crystallite size during calcination. The type of ZnO salt used as a precursor (acetate vs. nitrate) has no influence on the crystallographic parameters of the obtained photocatalysts.

N_2 isotherms and BJH pore-size distributions of the tested photocatalysts are illustrated in Figure 2, while their textural properties are summarized in Table 2.

N_2 adsorption–desorption isotherms, shown in the Figure 2, disclose the same type of hysteresis loop for all the examined photocatalyst samples. All isotherms represent the H3 type, the feature of textural structure with plate-like particles and slit-shaped pores. The observed hysteresis loop for all photocatalyst samples approaches $P/P_0 = 1$, denoting the presence of macropores (>50 nm). Regardless of the catalyst synthesis medium (water or ethanol), as the calcination temperature is increased from 300 °C to 700 °C, the BET surface area shows a decreasing trend as a result of the aggregation of the ZnO particles. The pronounced impact of the synthesis medium type on the pore size distribution can be observed. Namely, the water-originating samples show almost mono-modal pore size distributions, with the majority of pores located in the higher meso- and lower macro-range. Two peaks around 3 nm and 10 nm can be considered insignificant due to their low intensity. The sintering phenomenon, as a result of the increasing calcination temperature, is also reflected in the decrease in the average pore diameter and total pore volume for the

ZnO-NPs prepared from as water solution. Additionally, the substitution of the acetate precursor with nitrate does not contribute to the significant changes in textural characteristics. By examining the textural features of the ethanol-originating photocatalysts, it can be observed that these samples also undergo surface area and porosity decrease due to the calcination temperature impact, with the exception of the A_ZnOe_300 sample. This sample has a significantly higher portion of larger pores—narrower pore size distribution and higher values of porosity parameters—compared to its counterparts from both catalyst synthesis media. Figure 3 shows the SEM images of all ZnO-NPs prepared from water and ethanol solutions.
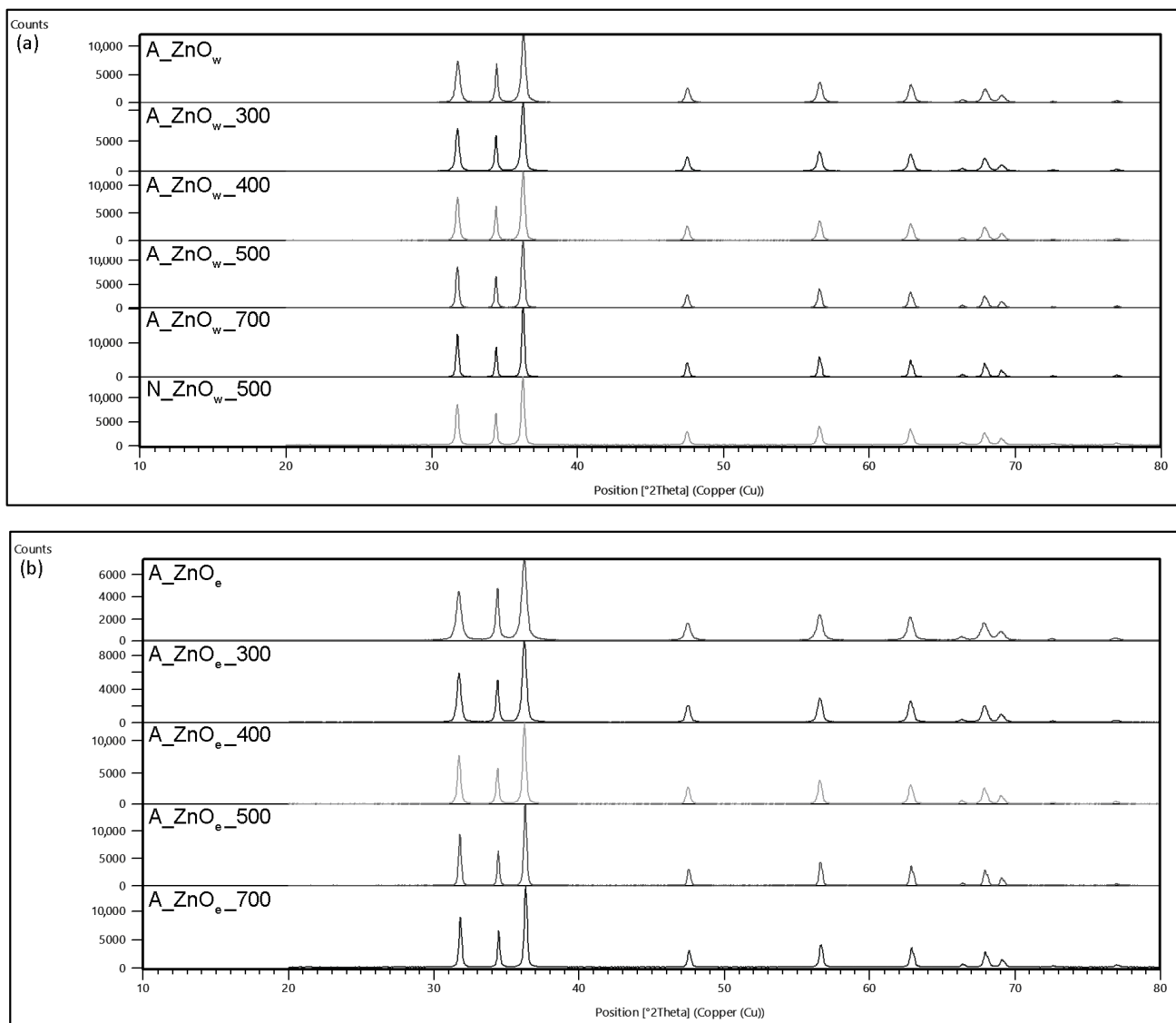

Figure 1. XRD patterns of ZnO-NPs prepared from (**a**) water and (**b**) ethanol solution.

Table 1. The average crystallite size of ZnO-NPs.

Photocatalyst Sample	Average Crystallite Size (nm)
A_ZnO$_w$	29.2
A_ZnO$_w$_300	31.9
A_ZnO$_w$_400	34.8
A_ZnO$_w$_500	40.1

Table 1. *Cont.*

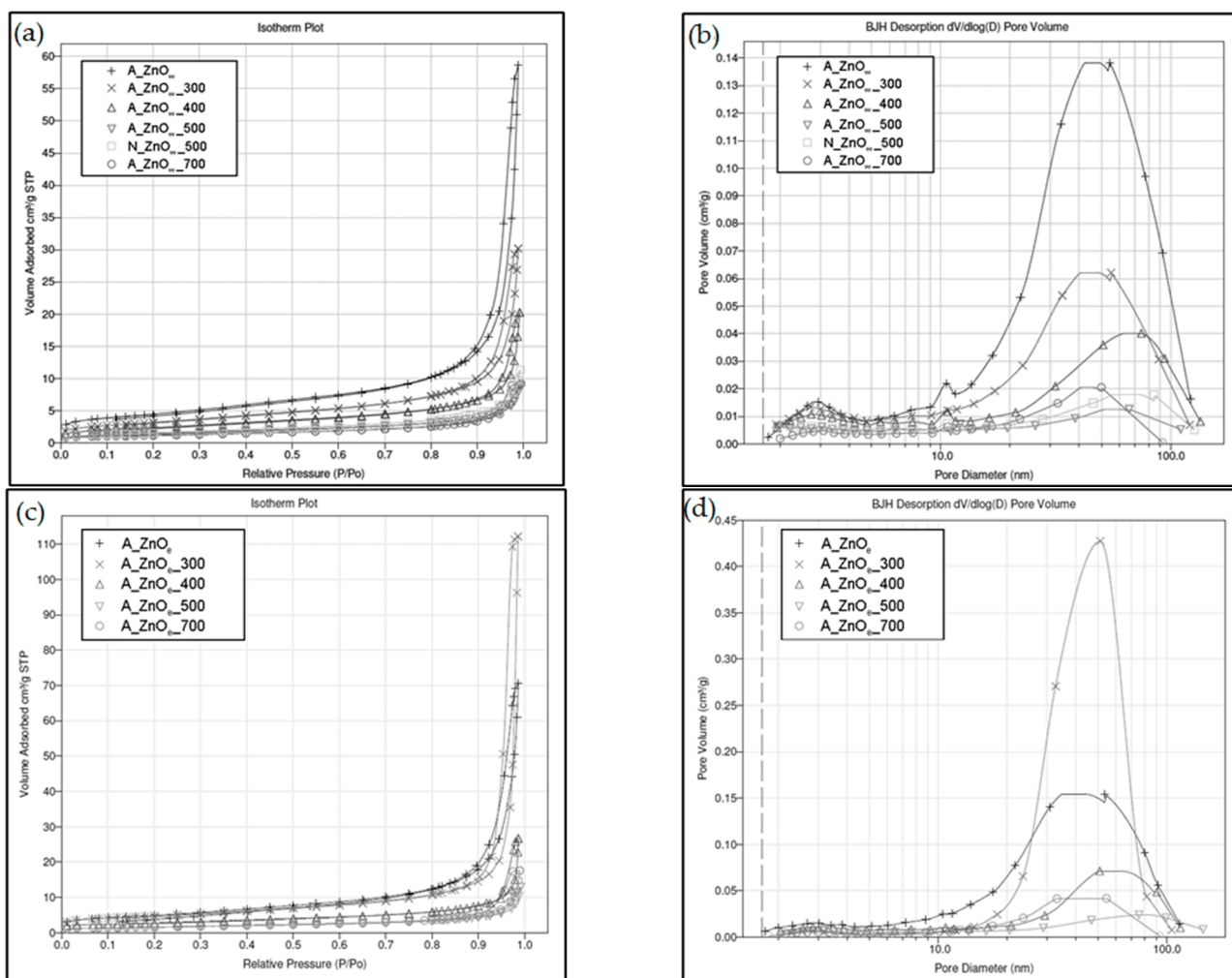| Photocatalyst Sample	Average Crystallite Size (nm)
N_ZnO$_w$_500	39.9
A_ZnO$_w$_700	45.1
A_ZnO$_e$	22.8
A_ZnO$_e$_300	27.8
A_ZnO$_e$_400	36.4
A_ZnO$_e$_500	45.9
A_ZnO$_e$_700	43.9

Figure 2. N$_2$ adsorption–desorption isotherms of ZnO-NPs prepared in (**a**) water and (**c**) ethanol solution and BJH pore size distribution of ZnO-NPs prepared in (**b**) water and (**d**) ethanol solution.

Table 2. Textural properties of ZnO photocatalysts.

Sample	Specific Surface Area (m²/g)	Average Pore Diameter (nm)	Total Pore Volume (cm³/g)
A_ZnO$_w$	15.80	21.0	0.091
A_ZnO$_w$_300	11.48	15.1	0.047

Table 2. *Cont.*

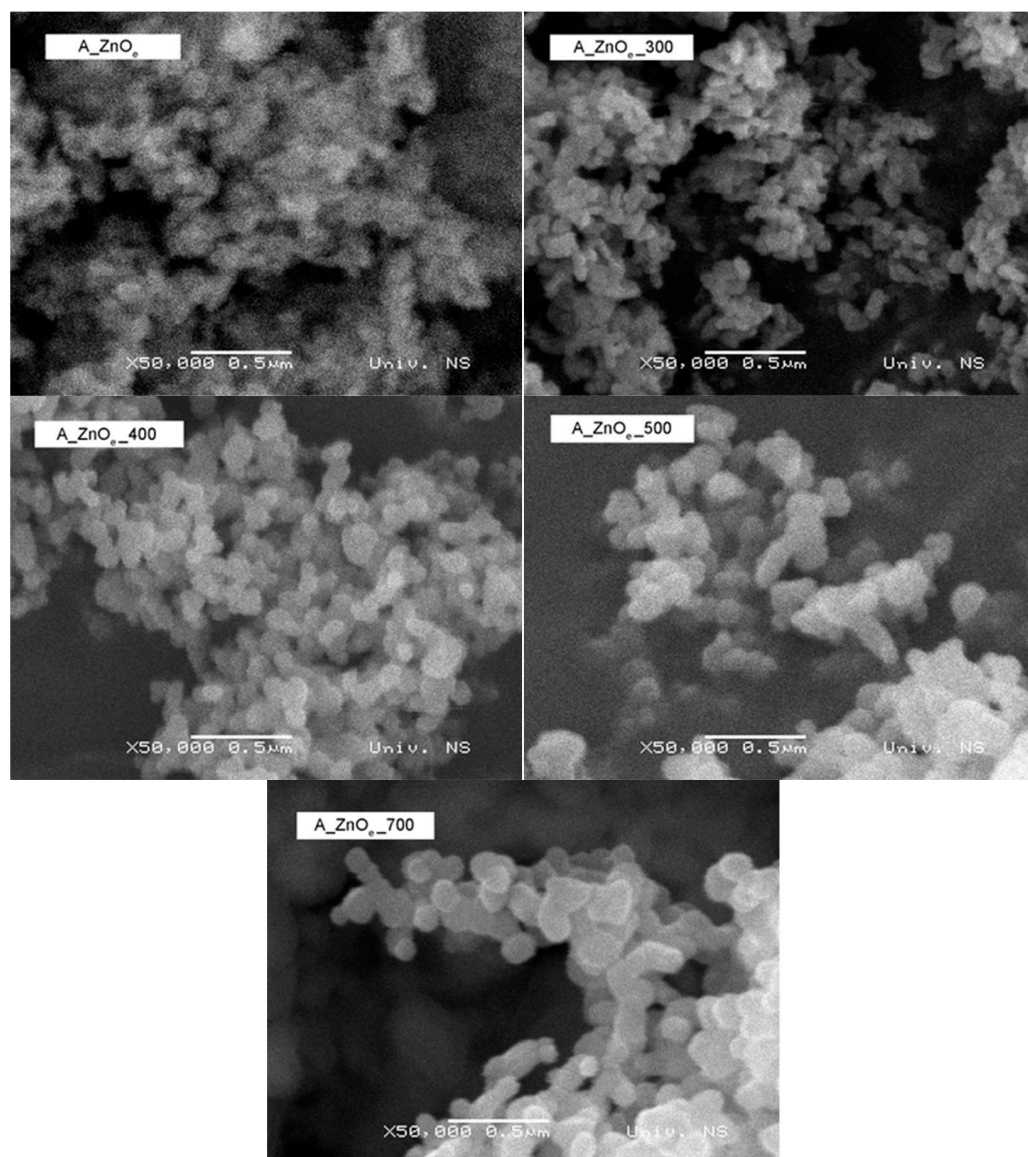| Sample	Specific Surface Area (m²/g)	Average Pore Diameter (nm)	Total Pore Volume (cm³/g)
A_ZnO$_w$_400	8.46	14.1	0.032
A_ZnO$_w$_500	5.21	10.3	0.014
N_ZnO$_w$_500	5.89	11.6	0.018
A_ZnO$_w$_700	4.08	13.7	0.014
A_ZnO$_e$	17.41	19.1	0.109
A_ZnO$_e$_300	17.04	34.8	0.174
A_ZnO$_e$_400	9.85	17.0	0.042
A_ZnO$_e$_500	5.67	14.7	0.020
A_ZnO$_e$_700	5.73	17.7	0.027
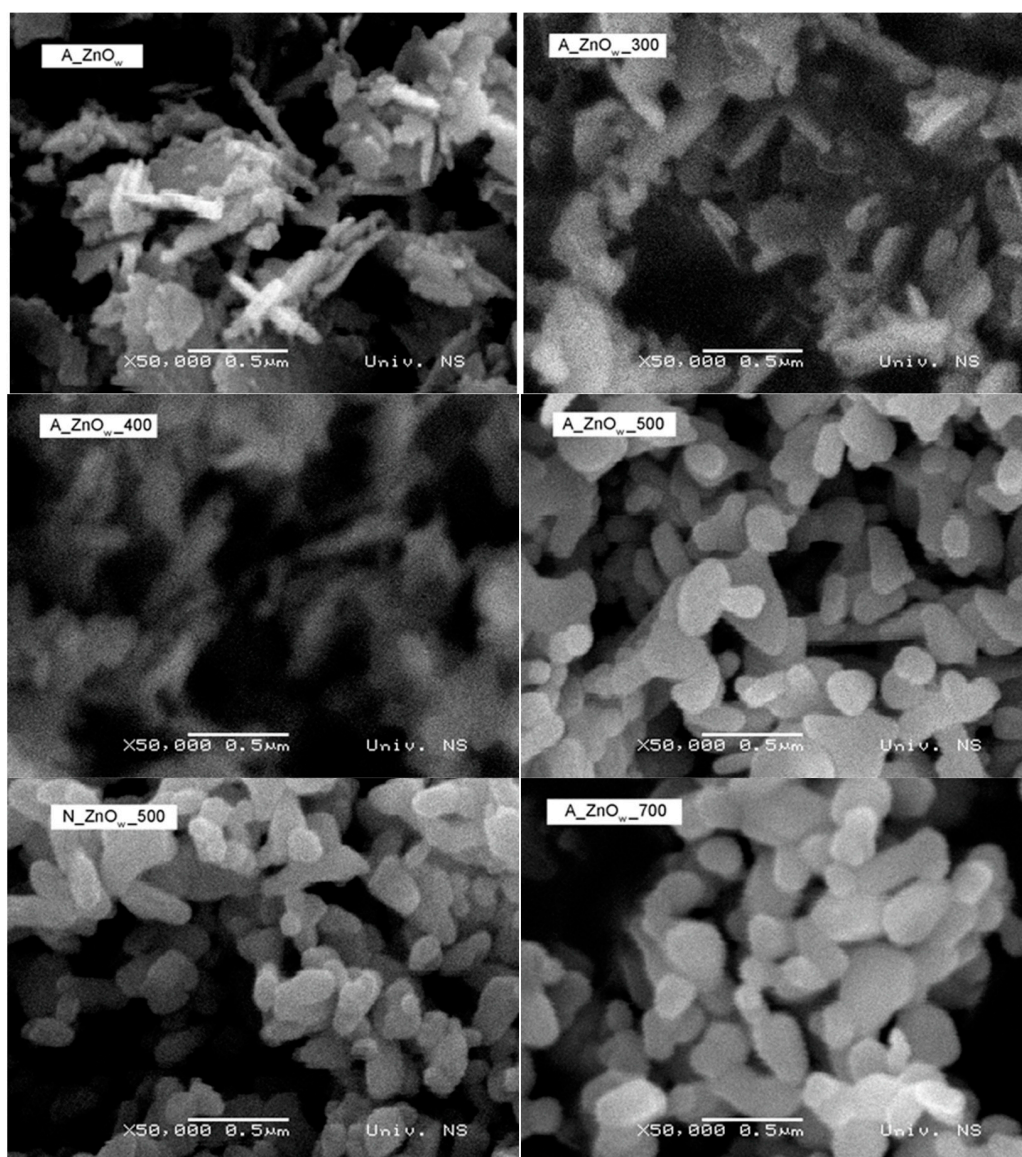
Figure 3. *Cont.*

Figure 3. SEM images of ZnO-NPs prepared from water and ethanol solutions.

The morphology of the prepared ZnO photocatalysts varies in relation to the applied calcination temperature, as well as the synthesis medium type (water vs. ethanol). Uncalcined, the A_ZnOw sample is composed of inhomogeneously defined nanoparticles, with most of them being irregularly shaped and overlapped. A certain amount of rod- shaped particles can also be observed in this sample. A similar morphology is maintained after calcination at 300 °C and 400 °C. The formation of regular, polyhedral nanoparticles with smooth edges can be associated with the higher calcination temperature, and the sintering phenomenon is especially pronounced upon calcination at 700 °C. The replacement of the acetate precursor with the nitrate one has no impact on the morphology of the final samples after their thermal treatment at the same temperature. Uncalcined, A_ZnOe is characterized by a different morphology compared to its water-originating counterpart. Namely, the observed particles are spherical and mutually connected in such a way as to form grape-like agglomerates. As the calcination temperature is increased, the overall morphology is mainly preserved, but due to the sintering phenomenon, the presence of individual, larger particles, still in the form of aggregates, is clearly visible.

3.2. Removal Efficiency

The efficacy of newly synthesized ZnO nanoparticles was investigated in the removal of the following pollutants: CLO, SUL, and AMI. The major cost associated with this process of using an expensive UV lamp was avoided using SS for solution irradiation. In order to examine the influence of the solvent type on the ZnO-NP photocatalytic performance, the ZnO photocatalysts were synthesized using water and ethanol solutions of two different metal precursors, followed by calcination at different temperatures. In order to compare the photocatalytic performance of ZnO-NPs, non-calcined ZnO-NPs were tested as well.

The removal kinetics of CLO and AMI under SS in the presence of the investigated ZnO-NPs are presented in Figure 4. In our previous investigations, we studied the photocatalytic degradation process of clomazone in the presence of TiO_2 powders [34,36]. However, in this study, we had the intention to analyze the influence of the ZnO-NP synthesis type on the photocatalytic activity in the degradation process of the mentioned pollutant. By comparing the kinetic curves in Figure 4a, it may be seen that by using A_ZnOw_300, A_ZnOw_400, A_ZnOw_500, and A_ZnOw_700, the efficiency of CLO removal was 41.6%, 52.8%, 50.2%, and 46.2%, respectively. On the other hand, without the calcination step, the efficiency of CLO removal was 27.4%. Under the same experimental conditions, practically no degradation of CLO was observed under SS in the absence of photocatalyst. Figure 4a shows the occurrence of the adsorption of CLO after 30 min of sonication in the dark, whereby the capacity of adsorption depends on the photocatalyst type. The highest adsorption (~31%) was found in the presence of A_ZnOw_400 (Figure 4a). However, in the case of A_ZnOw, A_ZnOw_300, A_ZnOw_500, and A_ZnOw_700 nanoparticles, lower adsorption was detected, namely 20.6%, 11.4%, 8.3%, and 3.5%, respectively. Based on the obtained data in Figure 4b, it can be seen that A_ZnOw_500 and A_ZnOw_700 nanoparticles showed similar behavior, and the highest efficiency of AMI removal was observed in their presence. The percentage of adsorption using A_ZnOw_700 was 29.5% after 30 min of sonication in the dark. On the other hand, catalysts A_ZnOw_500 and A_ZnOw_400 did not have an effect on the adsorption of AMI (Figure 4b). Based on the obtained data, it can be seen that among newly synthesized nanoparticles, A_ZnOw_500 had the highest efficiency for AMI removal, where after 60 min, 65% of the substrate was eliminated. On the other hand, based on our previous results of direct photolysis, after 60 min of degradation using SS, about 25% of the initial compound was removed [50].
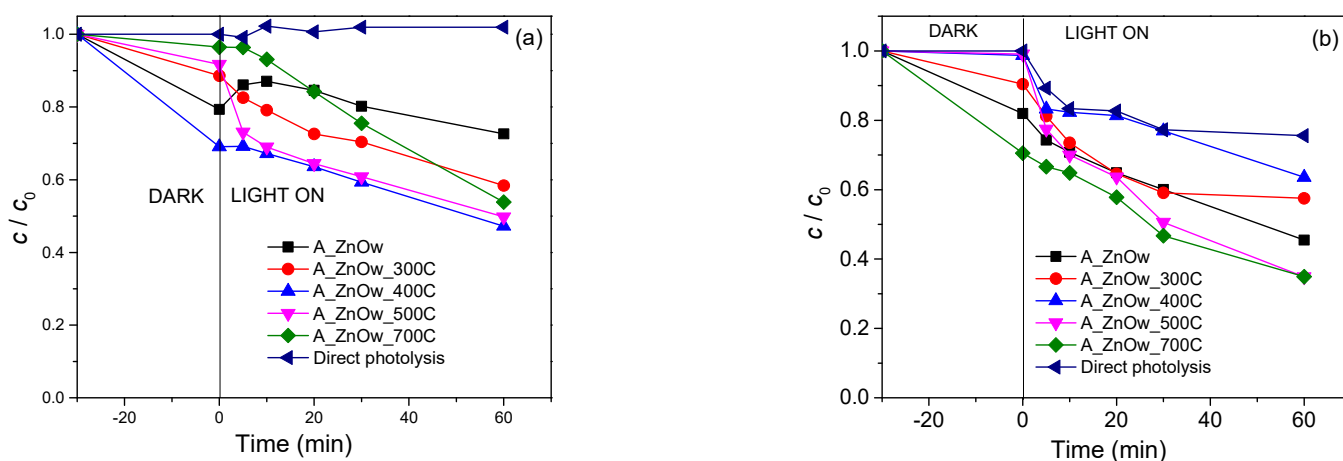

Figure 4. Kinetics of removal of (**a**) CLO and (**b**) AMI (0.03 mM) from water using A_ZnOw catalysts (1.0 mg/mL) under SS at pH ~7.

The previously described characterization results of ZnO-NPs prepared in water medium indicate that the obtained values of textural and XRD parameters coincide with the applied calcination temperature. On the other hand, by comparison with the morphology of ZnO-NPs, it can be suggested that these parameters cannot be considered

significant regarding photocatalytic activity, nor adsorption capacity in the dark, in the case of both CLO and AMI. Thus, a straightforward correlation between these properties and photocatalytic performance cannot be established. In the case of CLO removal from the water solution, the A_ZnOw_400 sample exhibits almost three-fold higher adsorption capacity during sonication in the dark compared to its counterpart previously calcined at 300 °C, while its photocatalytic activity is quite similar and moderately low. In contrast, after the thermal treatment of A_ZnOw at 500 °C and 700 °C, its adsorption capability in the absence of SS is negligible, whereas it further shows similar photocatalytic activity in the degradation of CLO, which is relatively higher compared to the A_ZnOw_300 and A_ZnOw_400 samples. These results suggest that the photoactivity, as well as the adsorption potential, can be closely related to the size and morphology of appropriate ZnO nanoparticles. Namely, as it can be seen from the SEM images, the calcination temperature of 500 °C can be designated as critical, signifying the complete change of particle morphology from rod-like shape particles to regular, polyhedral nanoparticles with smooth edges. Thus, the rod-like shape morphology of ZnO-NPs in the case of CLO removal can be considered inadequate in terms of both adsorption and photocatalytic performance, while the regular, polyhedral nanoparticles with smooth edges are more active in photocatalysis, revealing, on the other hand, a low adsorption capacity. Furthermore, the A_ZnOw_700 sample consists of larger particles (mostly in the form of aggregates) compared to A_ZnOw_500, resulting in different degradation kinetics for CLO, especially at the beginning of SS irradiation. The smaller particles in the A_ZnOw_500 sample favor faster photocatalytic performance during the first 10 min of the irradiation process. In the case of AMI removal, a similar trend for A_ZnOw_300 as for CLO was obtained, while the sample previously calcined at 400 °C exhibited rather low photoactivity, but almost no adsorption potential. The A_ZnOw_500 sample can also be distinguished as the best performing one for AMI removal. Additionally, contrasting the A_ZnOw_700 sample used for CLO degradation, the AMI molecules showed relatively high adsorption tendency in the dark toward these ZnO nanoparticles, while their photodegradation extent was lower. Based on previous observations, it can be suggested that in the case of water utilization as the catalyst synthesis medium, the formation of regular, polyhedral ZnO nanoparticles with smooth edges by applying the calcination temperature of 500 °C can be considered a prerequisite for minimizing the adsorption capacity in the dark for both CLO and AMI and favoring the photodegradation performance.

The results presented in Figure 5 show the percentage of adsorption and degradation of CLO and AMI in the presence of ZnO_e photocatalysts. In the presence of newly synthesized ZnO_e nanoparticles calcined at four different temperatures, the efficiency of CLO degradation was higher compared to uncalcined photocatalyst (Figure 5a). The catalytic activity of A_ZnOe_300 was the same as A_ZnOe_400 and higher than the other two calcined photocatalysts (A_ZnOe_500 and A_ZnOe_700); after 60 min of irradiation, about 55% of CLO was degraded. In contrast, the degradation efficiency of CLO differed to a lesser extent in the presence of A_ZnOe_500 and A_ZnOe_700, whereby the system with A_ZnOe_700 proved to be more efficient. Namely, in the presence of A_ZnOe_500 and A_ZnOe_700, 40.8% and 48.4% of CLO were respectively removed after 90 min of processing. Additionally, adsorption was also monitored on the investigated photocatalysts, and the following percentages were obtained: 14.15%, 31.31%, 34.72%, 30.1%, and 11.83%, in the case of A_ZnOe, A_ZnOe_300, A_ZnOe_400, A_ZnOe_500 and A_ZnOe_700, respectively (Figure 5a). The total removal efficacy of AMI in the presence of ZnOe photocatalysts was also examined, including both the adsorption and photodegradation process (Figure 5b). The percentages of adsorption and degradation in the presence of A_ZnOe, A_ZnOe_300, A_ZnOe_400, A_ZnOe_500, and A_ZnOe_700 were 56.27%, 49.39%, 48.70%, 53.22%, and 55.07% after 60 min of irradiation, respectively.
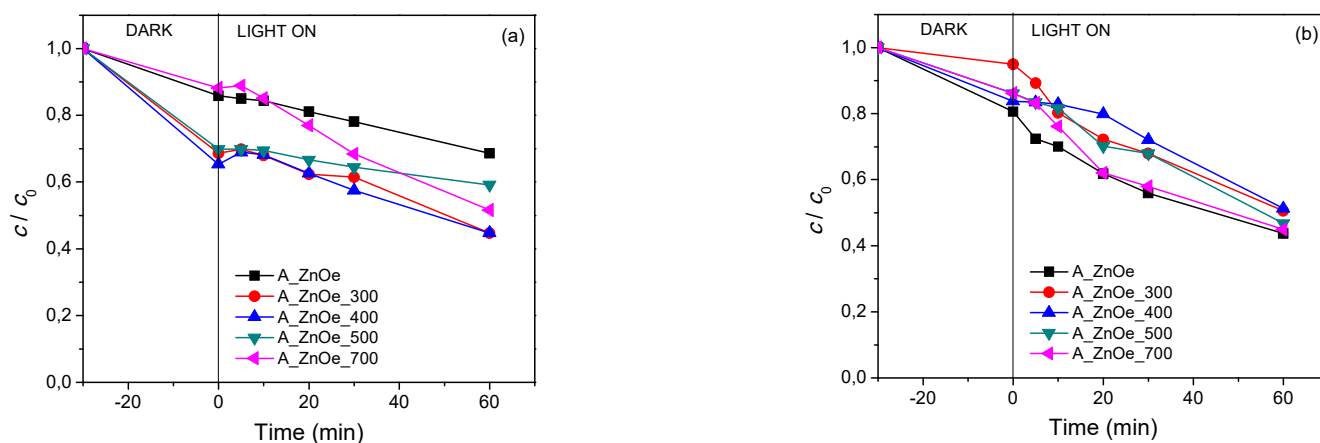
Figure 5. Kinetics of removal of (**a**) CLO and (**b**) AMI (0.03 mM) from water using A_ZnOe catalysts (1.0 mg/mL) under SS at pH ~7.

A_ZnO nanoparticles synthesized in ethanol medium are characterized by similar textural and XRD parameters to their water-originating counterpart, but they possess a different morphology in terms of both shape and size. They are more spherical and smaller with an enlargement trend following the increase in calcination temperature. A significant change of particle morphology was not observed by varying the calcination temperature, but A_ZnOe nanoparticles calcined at 700 °C have similar textural characteristics and average crystallite size to the ones produced by calcination at 500 °C. However, their performance in the process of CLO removal is different, and consequently can be related to the size of the particles. Larger particles (mostly in the form of grape-like aggregates) present in the A_ZnOe_700 sample can be regarded as the best candidate for achieving low adsorption potential in the dark and good photoactivity for CLO degradation. Other samples prepared at 300 °C, 400 °C, and 500 °C can be designated as inadequate for the overall performance in the mentioned process. In the case of AMI removal, smaller nanoparticles produced by calcination at 300 °C are favorable in terms of low adsorption capability in the absence of SS irradiation, while the application of other calcined A_ZnOe samples result in similar adsorption and photodegradation activity.

Additionally, the photocatalytic degradation efficiency of three different organic pollutants was compared due to the possibility that it is significantly affected by the molecular structure. Namely, A_ZnOw_500 was used in further experiments with SUL, due to its high efficiency in photodegradation processes and low adsorption capacities toward CLO and AMI. In addition, the photocatalytic activity of newly synthesized ZnO nanoparticles based on zinc–nitrate hexahydrate calcined at 500 °C (N_ZnOw_500) was investigated for CLO, AMI, and SUL removal in the presence of SS. Finally, the obtained results were compared with the system with A_ZnOw_500 (Figure 6). It can be concluded that the highest efficiency of elimination of CLO, AMI, and SUL was achieved in the systems with ZnO nanoparticles previously obtained from zinc–acetate hexahydrate as a precursor. In addition, the obtained results showed that the adsorption affinity of the substrates toward A_ZnOw_500 was lower compared to N_ZnOw_500.

The results of the physicochemical characterization of A_ZnOw_500 and N_ZnOw_500 revealed that there is no significant difference between their appropriate parameters indicating that the utilization of these two salts of Zn as precursors had almost no effect on the morphology, and textural and XRD parameters of the synthesized ZnO nanoparticles. On the other hand, they exhibited completely different performance in the examined processes of CLO, AMI and SUL removal, both in terms of adsorption potential in the dark and photoactivity under SS irradiation.
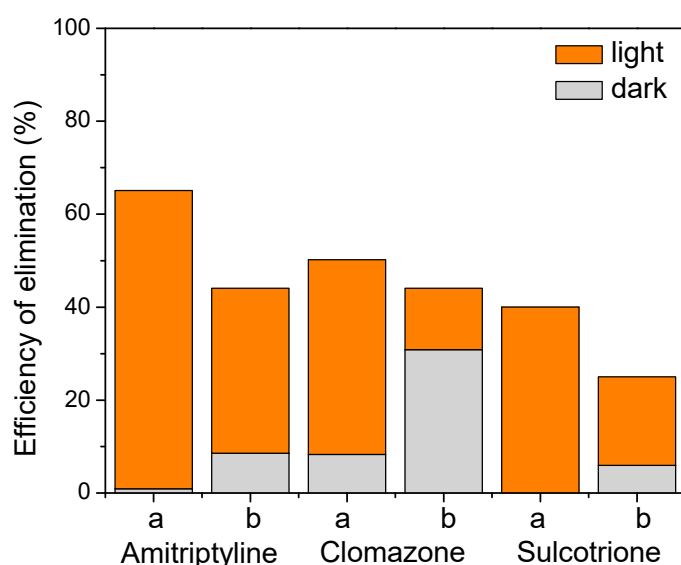
Figure 6. Efficiency of AMI, CLO, and SUL (0.03 mM) elimination from water using (**a**) A_ZnOw_500 and (**b**) N_ZnOw_500 catalysts (1.0 mg/mL) under SS.

Moreover, the influence of the initial pH value of the suspension of CLO, AMI, and SUL in the photocatalytic process was also studied. Namely, experiments were carried out in the presence of A_ZnOw_500, and the pH value was set at ~10. Apparent rate constants, k_{app}, with coefficient of determination, R^2, were calculated for pH ~7 and pH ~10. These results are given in Table 3. Based on the results, it was found that k_{app} was slightly increased in the range from pH ~7 to pH ~10 for the AMI removal. However, the pH value had no effect on the k_{app} value for the CLO and SUL removal. Our previous results obtained in the aqueous suspension of ZnO showed that at lower pH values ranging from 3 to 5, the photocatalytic degradation rate was the slowest as a consequence of ZnO dissolving in acidic media [51,52].

Table 3. Apparent rate constants (k_{app}) determined for 60 min irradiation using A_ZnOw_500. Results are expressed as mean $\pm$ SD of three independent experiments.

	k_{app} (min^{-1})	R^2	k_{app} (min^{-1})	R^2
		pH-Value		
Pollutant		~7		~10
CLO	0.0104	0.997	0.0100	0.999
AMI	0.0311	0.993	0.0398	0.929
SUL	0.0124	0.987	0.0116	0.995

4. Conclusions

In this research, firstly, the possible preparation of ZnO nanoparticles by the precipitation method was examined, as well as determining the structural and morphological properties of these powders using XRD, BET, and SEM techniques. In addition, the photocatalytic activity of the newly synthesized ZnO-NPs was also examined in the removal of selected organic pollutants, namely CLO, SUL, and AMI.

According to the data obtained about the photocatalytic efficiency of the newly synthesized NPs, it can be concluded that in the case of A_ZnOw catalysts, the highest performance was achieved after calcination at 400 °C for CLO and at 500 °C for AMI, while the non-calcined catalysts had lower efficiency. On the other hand, in the systems with A_ZnOe NPs, the highest removal of CLO was found to be after calcination at 500 °C, while in the case of AMI the non-calcined A_ZnOe had higher activity. This behavior can be explained

by the differences in the morphology of the different nanoparticles. Furthermore, our results also showed a moderate adsorption both in the presence of A_ZnOw and A_ZnOe. The activity of A_ZnOw_500 and N_ZnOw_500 catalysts in the removal of CLO, SUL, and AMI was also compared. Firstly, there were no differences found in the morphology. On the contrary, their activity was divergent in the removal of the selected pollutants. Namely, decreased photocatalytic activity was observed in the presence of N_ZnOw_500 NPs in all investigated systems. Finally, the effect of the initial pH was also examined. Based on our findings, it can be concluded that in the case of CLO and SUL, there was no influence of the initial pH found, while in the case of AMI the k_{app} was slightly increased in the range from pH ~7 to pH ~10.

References

1. Singh, J.; Rathi, A.; Rawat, M.; Kumar, V.; Kim, K.-H. The effect of manganese doping on structural, optical, and photocatalytic activity of zinc oxide nanoparticles. *Compos. Part B* **2019**, *166*, 361–370. [CrossRef]
2. Sabouni, R.; Gomaa, H. Photocatalytic degradation of pharmaceutical micro-pollutants using ZnO. *Environ. Sci. Pollut. Res. Int.* **2019**, *26*, 5372–5380. [CrossRef] [PubMed]
3. Fenner, K.; Canonica, S.; Wackett, L.P.; Elsner, M. Evaluating pesticide degradation in the environment: Blind spots and emerging opportunities. *Science* **2013**, *341*, 752–758. [CrossRef] [PubMed]
4. Buttiglieri, G.; Peschka, M.; Fromel, T.; Muller, J.; Malpei, F.; Seel, P.; Knepper, T.P. Environmental occurrence and degradation of the herbicide n-chloridazon. *Water Res.* **2009**, *43*, 2865–2873. [CrossRef]
5. Lu, M.; Du, J.; Zhou, P.; Chen, H.; Lu, C.; Zhang, Q. Endocrine disrupting potential of fipronil and its metabolite in reporter gene assays. *Chemosphere* **2015**, *120*, 246–251. [CrossRef] [PubMed]
6. Wang, X.; Yu, N.; Yang, J.; Jin, L.; Guo, H.; Shi, W.; Zhang, X.; Yang, L.; Yu, H.; Wei, S. Suspect and non-target screening of pesticides and pharmaceuticals transformation products in wastewater using QTOF-MS. *Environ. Int.* **2020**, *137*, 105599. [CrossRef] [PubMed]
7. Zhang, Q.; Ji, C.; Yan, L.; Lu, M.; Lu, C.; Zhao, M. The identification of the metabolites of chlorothalonil in zebrafish (Danio rerio) and their embryo toxicity and endocrine effects at environmentally relevant levels. *Environ. Pollut.* **2016**, *218*, 8–15. [CrossRef] [PubMed]
8. Hensen, B.; Olsson, O.; Kummerer, K. A strategy for an initial assessment of the ecotoxicological effects of transformation products of pesticides in aquatic systems following a tiered approach. *Environ. Int.* **2020**, *137*, 105533. [CrossRef] [PubMed]
9. Le Cor, F.; Slaby, S.; Dufour, V.; Iuretig, A.; Feidt, C.; Dauchy, X.; Banas, D. Occurrence of pesticides and their transformation products in headwater streams: Contamination status and effect of ponds on contaminant concentrations. *Sci. Total Environ.* **2021**, *788*, 147715. [CrossRef]
10. Zanella, R.; Primel, E.G.; Machado, S.L.O.; Gonçalves, F.F.; Marchezan, E. Monitoring of the herbicide clomazone in environmental water samples by solid-phase extraction and high-performance liquid chromatography with ultraviolet detection. *Chromatographia* **2002**, *55*, 573–577. [CrossRef]

11. Zanella, R.; Primel, E.G.; Gonçalves, F.F.; Martins, M.L.; Adaime, M.B.; Marchesan, E.; Machado, S.L.O. Study of the degradation of the herbicide clomazone in distilled and in irrigated rice field waters using HPLC-DAD and GC-MS. *J. Braz. Chem. Soc.* **2008**, *19*, 987–995. [CrossRef]

12. de Menezes, C.C.; Loro, V.L.; da Fonseca, M.B.; Cattaneo, R.; Pretto, A.; Miron, D.d.S.; Santi, A. Oxidative parameters of Rhamdia quelen in response to commercial herbicide containing clomazone and recovery pattern. *Pestic. Biochem. Physio.* **2011**, *100*, 145–150. [CrossRef]

13. Bonnet, J.L.; Bonnemoy, F.; Dusser, M.; Bohatier, J. Toxicity assessment of the herbicides sulcotrione and mesotrione toward two reference environmental microorganisms: Tetrahymena pyriformis and Vibrio fischeri. *Arch. Environ. Contam. Toxicol.* **2008**, *55*, 576–583. [CrossRef] [PubMed]

14. Cherrier, R.; Boivin, A.; Perrin-Ganier, C.; Schiavon, M. Sulcotrione versus atrazine transport and degradation in soil columns. *Pest. Manag. Sci.* **2005**, *61*, 899–904. [CrossRef]

15. Chaabane, H.; Cooper, J.-F.; Azouzi, L.; Coste, C.-M. Influence of soil properties on the adsorption−desorption of sulcotrione and its hydrolysis metabolites on various soils. *J. Agric. Food Chem.* **2005**, *53*, 4091–4095. [CrossRef]

16. EFSA European Food Safety Authority. Conclusion regarding the peer review of the pesticide risk assessment of the active substance of sulcotrione. *EFSA Sci. Rep.* **2008**, *150*, 1–86.

17. Barchanska, H.; Sajdak, M.; Szczypka, K.; Swientek, A.; Tworek, M.; Kurek, M. Atrazine, triketone herbicides, and their degradation products in sediment, soil and surface water samples in Poland. *Environ. Sci. Pollut. Res. Int.* **2017**, *24*, 644–658. [CrossRef]

18. Simazaki, D.; Kubota, R.; Suzuki, T.; Akiba, M.; Nishimura, T.; Kunikane, S. Occurrence of selected pharmaceuticals at drinking water purification plants in Japan and implications for human health. *Water Res.* **2015**, *76*, 187–200. [CrossRef] [PubMed]

19. Verlicchi, P.; Al Aukidy, M.; Zambello, E. Occurrence of pharmaceutical compounds in urban wastewater: Removal, mass load and environmental risk after a secondary treatment—A review. *Sci. Total Environ.* **2012**, *429*, 123–155. [CrossRef]

20. World Health Organization. *Pharmaceuticals in Drinking-Water*; World Health Organization: Geneva, Switzerland, 2013. Available online: https://www.who.int/publications/m/item/information-sheet-pharmaceuticals-in-drinking-water (accessed on 6 October 2022).

21. Schultzt, M.M.; Furlong, E.T. Trace analysis of antidepressant pharmaceuticals and their select degradates in aquatic matrixes by LC/ESI/MS/MS. *Anal. Chem.* **2003**, *80*, 1756–1762. [CrossRef]

22. Calisto, V.; Esteves, V.I. Psychiatric pharmaceuticals in the environment. *Chemosphere* **2009**, *77*, 1257–1274. [CrossRef]

23. Abbar, J.C.; Lamani, S.D.; Nandibewoor, S.T. Ruthenium(III) catalyzed oxidative degradation of amitriptyline-A tricyclic antidepressant drug by permanganate in aqueous acidic medium. *J. Sol. Chem.* **2011**, *40*, 502–520. [CrossRef]

24. Kasprzyk-Hordern, B.; Dinsdale, R.M.; Guwy, A.J. Multiresidue methods for the analysis of pharmaceuticals, personal care products and illicit drugs in surface water and wastewater by solid-phase extraction and ultra performance liquid chromatography–electrospray tandem mass spectrometry. *Anal. Bioanal. Chem.* **2008**, *391*, 1293–1308. [CrossRef]

25. Lajeunesse, A.; Gagnon, C.; Sauvé, S. Determination of basic antidepressants and their N-desmethyl metabolites in raw sewage and wastewater using solid-phase extraction and liquid chromatography−tandem mass spectrometry. *Anal. Chem.* **2008**, *80*, 5325–5333. [CrossRef]

26. Kasprzyk-Hordern, B.; Dinsdale, R.M.; Guwy, A.J. The occurrence of pharmaceuticals, personal care products, endocrine disruptors and illicit drugs in surface water in South Wales, UK. *Water Res.* **2008**, *42*, 3498–3518. [CrossRef] [PubMed]

27. Vystavna, Y.; Huneau, F.; Grynenko, V.; Vergeles, Y.; Celle-Jeanton, H.; Tapie, N.; Budzinski, H.; Le Coustumer, P. Pharmaceuticals in rivers of two regions with contrasted socio-economic conditions: Occurrence, accumulation, and comparison for Ukraine and France. *Water Air Soil Pollut.* **2012**, *223*, 2111–2124. [CrossRef]

28. Togola, A.; Budzinski, H. Multi-residue analysis of pharmaceutical compounds in aqueous samples. *J. Chromatogr. A* **2008**, *1177*, 150–158. [CrossRef] [PubMed]

29. Bhatkhande, D.S.; Pangarkar, V.G.; Beenackers, A.A.C.M. Photocatalytic degradation for environmental applications—A review. *J. Chem. Technol. Biotechnol.* **2002**, *77*, 102–116. [CrossRef]

30. Kumar, M.; Mehta, A.; Mishra, A.; Singh, J.; Rawat, M.; Basu, S. Biosynthesis of tin oxide nanoparticles using Psidium Guajava leave extract for photocatalytic dye degradation under sunlight. *Mater. Lett.* **2018**, *215*, 121–124. [CrossRef]

31. Benitez, F.J.; Acero, J.L.; Real, F.J.; Roldan, G.; Casas, F. Comparison of different chemical oxidation treatments for the removal of selected pharmaceuticals in water matrices. *Chem. Eng. J.* **2011**, *168*, 1149–1156. [CrossRef]

32. Musial, J.; Mlynarczyk, D.T.; Stanisz, B.J. Photocatalytic degradation of sulfamethoxazole using TiO_2-based materials—Perspectives for the development of a sustainable water treatment technology. *Sci. Total Environ.* **2023**, *856*, 159122. [CrossRef]

33. Zhang, Y.; Zhou, B.; Chen, H.; Yuan, R. Heterogeneous photocatalytic oxidation for the removal of organophosphorus pollutants from aqueous solutions: A review. *Sci. Total Environ.* **2023**, *856*, 159048. [CrossRef]

34. Abramovic, B.F.; Despotovic, V.N.; Sojic, D.V.; Orcic, D.Z.; Csanadi, J.J.; Cetojevic-Simin, D.D. Photocatalytic degradation of the herbicide clomazone in natural water using TiO_2: Kinetics, mechanism, and toxicity of degradation products. *Chemosphere* **2013**, *93*, 166–171. [CrossRef]

35. Šojić, D.V.; Orčić, D.Z.; Četojević-Simin, D.D.; Banić, N.D.; Abramović, B.F. Efficient removal of sulcotrione and its formulated compound Tangenta® in aqueous TiO$_2$ suspension: Stability, photoproducts assessment and toxicity. *Chemosphere* **2015**, *138*, 988–994. [CrossRef]

36. Šojić Merkulov, D.V.; Despotović, V.D.; Banić, N.D.; Armaković, S.J.; Finčur, N.L.; Lazarević, M.J.; Četojević-Simin, D.D.; Orčić, D.Z.; Radoičić, M.B.; Šaponjić, Z.V.; et al. Photocatalytic decomposition of selected biologically active compounds in environmental waters using TiO$_2$/polyaniline nanocomposites: Kinetics, toxicity and intermediates assessment. *Environ. Pollut.* **2018**, *239*, 457–465. [CrossRef]

37. Khan, M.M.; Adil, S.F.; Al-Mayouf, A. Metal oxides as photocatalysts. *J. Saudi. Chem. Soc.* **2015**, *19*, 462–464. [CrossRef]

38. Carraway, E.R.; Hoffman, A.J.; Hoffmann, M.R. Photocatalytic oxidation of organic-acids on quantum-sized semiconductor colloids. *Environ. Sci. Technol.* **1994**, *28*, 786–793. [CrossRef] [PubMed]

39. Pal, B.; Sharon, M. Enhanced photocatalytic activity of highly porous ZnO thin films prepared by sol-gel process. *Mater. Chem. Phys.* **2002**, *76*, 82–87. [CrossRef]

40. Chang, X.; Li, Z.; Zhai, X.; Sun, S.; Gu, D.; Dong, L.; Yin, Y.; Zhu, Y. Efficient synthesis of sunlight-driven ZnO-based heterogeneous photocatalysts. *Mater. Des.* **2016**, *98*, 324–332. [CrossRef]

41. Zhu, Y.; Xu, G.; Guo, T.; Hou, H.; Tan, S. Preparation, infrared emissivity and thermochromic properties of Co doped ZnO by solid state reaction. *J. Alloys Compd.* **2017**, *720*, 105–115. [CrossRef]

42. Kakarndee, S.; Nanan, S. SDS capped and PVA capped ZnO nanostructures with high photocatalytic performance toward photodegradation of reactive red (RR141) azo dye. *J. Environ. Chem. Eng.* **2018**, *6*, 74–94. [CrossRef]

43. Jia, P.; Tan, H.; Liu, K.; Gao, W. Enhanced photocatalytic performance of ZnO/bone char composites. *Mater. Lett.* **2017**, *205*, 233–235. [CrossRef]

44. Mahdavi, R.; Talesh, S.S.A. Sol-gel synthesis, structural and enhanced photocatalytic performance of Al doped ZnO nanoparticles. *Adv. Powder Technol.* **2017**, *28*, 1418–1425. [CrossRef]

45. Phuruangrat, A.; Thongtem, S.; Thongtem, T. Ultrasonic-assisted synthesis and photocatalytic performance of ZnO nanoplates and microflowers. *Mater. Des.* **2016**, *107*, 250–256. [CrossRef]

46. Arsha Kusumam, T.V.; Panakkal, T.; Divya, T.; Nikhila, M.P.; Anju, M.; Anas, K.; Renuka, N.K. Morphology controlled synthesis and photocatalytic activity of zinc oxide nanostructures. *Ceram. Inter.* **2016**, *42*, 3769–3775. [CrossRef]

47. Mohd Daud, S.N.H.; Haw, C.; Chiu, W.; Aspanut, Z.; Chia, M.; Khanis, N.H.; Khiew, P.; Abd Hamid, M.A. ZnO nanonails: Organometallic synthesis, self-assembly and enhanced hydrogen gas production. *Mater. Sci. Semicond. Process.* **2016**, *56*, 228–237. [CrossRef]

48. Lowell, S.; Shields, J.E.; Thomas, M.A.; Thommes, M. *Characterization of Porous Solids and Powders: Surface Area, Pore Size and Density*; Kluwer Academic Publishers: Dordrecht, The Netherlands; Boston, MA, USA; London, UK, 2004. [CrossRef]

49. Lente, G. *Deterministic Kinetics in Chemistry and Systems Biology the Dynamics of Complex Reaction Networks*; Springer: Berlin/Heidelberg, Germany, 2015. [CrossRef]

50. Finčur, N.; Šojić Merkulov, D.; Putnik, P.; Despotović, V.; Banić, N.; Lazarević, M.; Četojević-Simin, S.; Agbaba, J.; Abramović, B. Environmental photocatalytic degradation of antidepressants with solar radiation: Kinetics, mineralization, and toxicity. *Nanomaterials* **2021**, *11*, 632. [CrossRef] [PubMed]

51. Finčur, N.L.; Krstić, J.B.; Šibul, F.S.; Šojić, D.V.; Despotović, V.N.; Banić, N.D.; Agbaba, J.R.; Abramović, B.F. Removal of alprazolam from aqueous solutions by advanced oxidation processes: Influencing factors, intermediates, and products. *Chem. Eng. J.* **2017**, *307C*, 1105–1115. [CrossRef]

52. Šojić, D.V.; Orčić, D.Z.; Četojević-Simin, D.D.; Despotović, V.D.; Abramović, B.F. Kinetics and the mechanism of the photocatalytic degradation of mesotrione in aqueous suspension and toxicity of its degradation mixtures. *J. Mol. Catal. A Chem.* **2014**, *392*, 67–75. [CrossRef]